Proceedings of IMECE 2005
2005 ASME International Mechanical Engineering Congress & Exposition
Orlando, USA, November 5-11, 2005

DRAFT **IMECE2005-82993**

MONTE CARLO SCHEMES FOR RADIATIVE TRANSFER IN MEDIA REPRESENTED BY PARTICLE FIELDS

Anquan Wang
Department of Mechanical Engineering
Pennsylvania State University
University Park, Pennsylvania 16802
Email: aqwang@psu.edu

Michael F. Modest*
Department of Mechanical Engineering
Pennsylvania State University
University Park, Pennsylvania 16802
Email: mfm6@psu.edu

ABSTRACT

Monte Carlo ray-tracing schemes are developed for the evaluation of radiative heat transfer for problems, in which the participating medium is represented by discrete point-masses, such as the flow field and scalar fields in PDF Monte Carlo methods frequently used in combustion modeling. Photon ray tracing in such cases requires that an optical thickness is assigned to each of the point-masses. Two approaches are discussed, the Point Particle Model (PPM), in which the shape of particle is not specified, and the Spherical Particle Model (SPM) in which particles are assumed to be spheres with constant radiation properties. Another issue for ray tracing in particle fields is the influence region of a ray. Two ways of modeling a ray are proposed. In the first, each ray is treated as a standard volume-less line. In the other approach, the ray is assigned a small solid angle, and is thus treated as a cone with a decaying influence function away from its center line. Based on these models, three different interaction schemes between rays and particles are proposed, i.e., Line-SPM, Cone-PPM and Cone-SPM methods, and are compared employing several test problems.

Nomenclature

A	cylindrical shell
I	emission intensity; particles enclosed by ray
L	thickness of gas slab; side-length of computational domain
Q_{emi}	total energy emitted from a particle
R	particle influence radius; gas constant
R_c	local radius of cone
T	temperature
V_o	nominal volume of particle
W	weight function
m	particle mass
p	total pressure
q	heat flux
r	distance to axis of conical ray
r'	normalized distance to ray axis, r/R_c
s	axial distance from emission point
$\mathbf{x}$	location vector
Ω	particle influence region
Ω'	particle influence region intercepted by ray
κ	linear absorption coefficient
κ_ρ	density-based absorption coefficient
η	random number
ρ_o	nominal density of particle
$\hat{\rho}$	density profile in particle influence region
τ	optical thickness
superscript	
$'$	quantity normalized by local cone radius R_c
subscripts	
i	particle
j	ray
2D, 3D	dimension of weight function

*Address all correspondence to this author.

1 Introduction

Among radiative transfer models, Monte Carlo Ray Tracing (MCRT) has several advantages over other popular models, because it can be applied to problems of arbitrary difficulty with relative ease [1]. The MCRT method directly simulates the physical processes, i.e., emission, absorption, scattering and reflection, from which the Radiative Transfer Equation (RTE) is derived. In the standard Monte Carlo method, a ray carrying a fixed amount of energy is emitted and its progress is then traced until it is absorbed at a certain point in the participating medium or on the wall, or until it escapes from the enclosure. As many researchers have pointed out [2–6], this method is inefficient when the walls are highly reflective and/or the medium is optically thin so that most photon bundles exit the enclosure without any contribution. Modest [4, 5] applied the concept of energy partitioning to alleviate this problem. In this method the energy carried by a ray is no longer fixed along the path and absorbed once and for all at one point, but rather is attenuated gradually along the path until its depletion or until it leaves the enclosure. The locally absorbed fraction of the ray's energy contributes to the heat exchange rates of sub-volumes along the ray path. This method is also called "absorption suppression" by Walters and Buckius [6]. A large variety of problems of great complexity can be simulated with a reasonable efficiency using either standard or energy partition methods in forward Monte Carlo simulations, when the overall knowledge of the radiation field is desired. However, such scheme can be very inefficient if only the radiative intensity hitting a small spot and/or over a small range of solid angle is required. The idea of backward tracing, which only traces the rays that eventually hit the targeted area or solid angle, has been proposed by several researchers in different topics to handle this inefficiency. The comprehensive formulation for backward Monte Carlo simulations in radiative heat transfer can be found in the literature (Walters and Buckius [6], Modest [7]).

The MCRT method has been applied to all aspects of radiative heat transfer [8, 9]. In applications, in which no participating medium is involved, ray tracing is relatively simple. However, in many high-temperature applications, such as combustion problems, participating media play a key role. A major difficulty is the evaluation of the optical thickness that a ray passes through, since the temperature and concentration fields are highly inhomogeneous. In their Monte Carlo modeling of radiative heat transfer in turbulent flames, Tessé and coworkers [10, 11] assumed uniform properties of the medium along the integral length of each coherent turbulence structure crossed by the ray, in order to determine the optical thickness along the ray's path. However, in other problems, in which the participating medium is represented by the field of point-masses, such as the flow field and scalar fields in PDF Monte Carlo methods [12–15] frequently used in combustion modeling, the above continuum model is no longer useful. No work appears to have been done to date to implement MTRC in discrete particle fields, which is the aim of the present work.

2 Ray-Particle Interaction Models

To simulate the radiative transfer process by ray tracing in a discrete particle field, the interaction between infinitesimal point-masses and infinitesimally thin photon rays needs to be modeled. This can be done by assigning effective volumes to the point-masses, by assigning an influence volume to the ray's trajectory, or a combination of both. In this section, several particle models and ray models are developed first, followed by photon emission and absorption algorithms based on these models.

2.1 Modeling Discrete Particles and Photon Rays

Point Particle Model (PPM) In this model, particles are treated as point-masses, i.e., they carry an amount of mass without a specific shape at a certain spatial location as shown in Fig. 1a which is a 2D particle field. The only geometric information known about the particles is their position vector. However, particles do have a nominal volume, which may be calculated from their thermophysical properties such as pressure and temperature. For example, if the ideal gas assumption is adopted, the nominal volume may be computed as

$$V_{o,i} = \frac{m_i R T_i}{p_i}, \tag{1}$$

where m_i is the mass carried by particle i, T_i is its temperature, p_i is its total pressure and R is the gas constant. To enforce consistency in the discrete particle representation of the medium, the overall nominal volume of all particles should be the same as the actual geometric expanse of the medium. Therefore, we may regard the nominal volume of a particle as its real volume.

The Point Particle Model only contains the particle information that the original discrete particle field contains. It does not employ any other assumption. Therefore, it will not induce any inconsistency that further assumptions may have. The disadvantage of this model is that it is difficult to interact a photon ray with a volume without shape.

Spherical Particle Model In this method, each point-mass m_i has a spherical influence region Ω_i, surrounding it as shown in Fig. 1b. The mass is distributed to its influence region according to a density profile,

$$\hat{\rho}_i(\mathbf{x}) = \begin{cases} \rho_{o,i} W_{3D}\left(\dfrac{|\mathbf{x}-\mathbf{x}_i|}{R_i}\right), & |\mathbf{x}-\mathbf{x}_i| < R_i \\ 0, & |\mathbf{x}-\mathbf{x}_i| \geq R_i \end{cases}, \tag{2}$$

where $\mathbf{x}_i$ is the spatial location vector of the point-mass i, R_i is

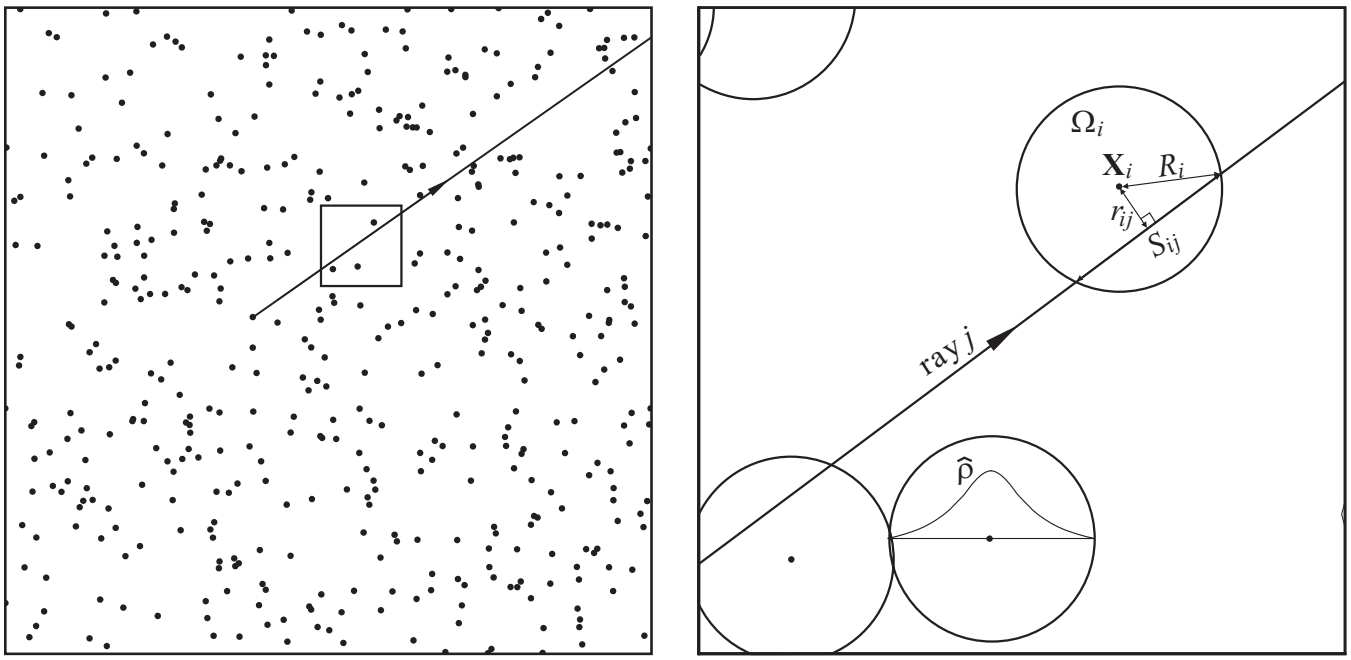

Figure 1. (a) PPM representation of a medium; (b) SPM/CDS representation of a sub-region in (a)

its influence radius, $\rho_{o,i}$ is the nominal density calculated by

$$\rho_{o,i} = \frac{m_i}{V_{o,i}} = \frac{p_i}{RT_i}, \tag{3}$$

and W_{3D} is a spherically symmetric weight function which decays from the center along radial directions and satisfies the following condition,

$$\int_{\Omega_i} W_{3D}\left(\frac{|\mathbf{x}-\mathbf{x}_i|}{R_i}\right) \mathrm{d}\mathbf{x} = V_{o,i}, \tag{4}$$

so that the total mass in the influence region is equal to the point-mass. In this method, particles are assigned a spherical volume (influence region) with varying density, and overlapping other particles in the domain. This is called the Spherical Particle Method (SPM).

One may adjust the size of influence region and the mass distribution of particles by employing different weight functions. Larger influence radii lead to more particle overlap and spatial gradients may be smoothed out. On the other hand, Smaller influence radii result in smaller particle volumes, making it more difficult to interact with rays. The simplest possible weight function is

$$W_{3D}\left(\frac{|\mathbf{x}-\mathbf{x}_i|}{R_i}\right) = 1, \tag{5}$$

i.e., the density is constant in the influent region and its volume is the same as the nominal volume of the particle. The particles can then be regarded as constant density spheres with a radius determined by their nominal volumes,

$$R_i = \left(\frac{3V_{o,i}}{4\pi}\right)^{1/3}. \tag{6}$$

This model will be termed the Constant Density Sphere (CDS) model. The overall density at an arbitrary position is the sum of density contributions from all nearby particles. Some locations may be influenced by more than one particle, while some other locations may not be in the influence region of any particle, i.e., there is a void in these places. Therefore, this model cannot recover the continuous density medium as shown in Fig. 1b and Fig. 2. Figure 1b is a small portion of the CDS representation of the 2D field given in Fig. 1a (if variable density were employed, the R_i would be larger, resulting in substantial overlap, even in this region of few paticles). A location with lots of void space was chosen for simplicity in Fig. 1b, and in order to show particle locations in a plane, a 2D rather than 3D particle field is depicted in Fig. 1. Figure 2 shows the density distribution on a cross-section of a 3D CDS representation of a homogeneous medium.

Line Ray Model In this model, a ray is simply treated as a volume-less line and energy propagates one-dimensionally along

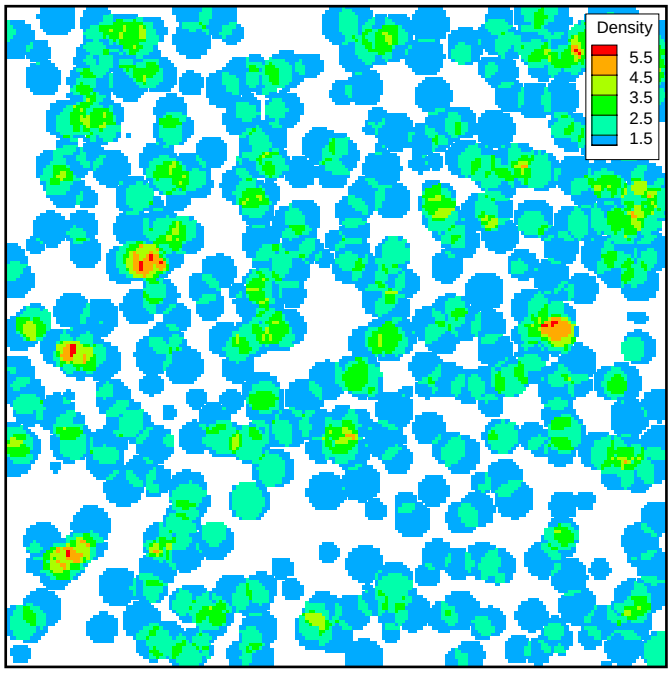

Figure 2. Density distribution of a CDS representation for a homogeneous medium

the line. This is the standard model for ray tracing in continuous media. Since such rays are not designed to have a specific volume, they are not able to interact with point-masses. Therefore, this model requires volumetric particle models for radiative transfer simulations.

Cone Ray Model Physically, a photon bundle consists of many millions of individual photons, occupying a small solid angle. Thus, to model the volume of a ray, we assign a small solid angle to the ray and treat it as a cone. Energy is assumed to propagate axisymmetrically in two dimensions, with its strength decaying in the radial direction normal to the cone axis, similar to the weight function assigned to particle density in Eq. (2) but in 2D. For a ray emitted at $\mathbf{x}_o$ into a direction given by a unit direction vector $\hat{\mathbf{s}}$, the intensity at location $\mathbf{x}$ in the ray can be modeled as

$$I(s,r) = I_o(s) W_{2D}(r/R_c(s)), \tag{7}$$

where $s = (\mathbf{x} - \mathbf{x}_o) \cdot \hat{\mathbf{s}}$ is the distance from the emission location to a point on the ray axis, r is the distance from a point on a plane normal to the ray axis, $I_o(s)$ is the intensity at the ray center, and $R_c(s)$ is the local influence radius of the cross-section as depicted in Fig. 3. W_{2D} is a normalized two-dimensional center-symmetric profile which satisfies

$$\int_0^1 W_{2D}(r') 2r' \, \mathrm{d}r' = 1 \quad \text{and} \quad r' = r/R_c. \tag{8}$$

Again, many weight functions are possible, ranging from $W_{2D} = 1$ to Gaussian decay. A popular Gaussian-like weight function is provided here [16] as

$$W_{2D}(r') = \frac{60}{7} \begin{cases} \frac{1}{3} - 4r'^2 + 4r'^3, & 0 \le r' < \frac{1}{2} \\ \frac{4}{3}(1-r')^3, & \frac{1}{2} \le r' < 1 \\ 0, & r' \ge 1 \end{cases}. \tag{9}$$

Since in this model the ray has a specific volume, volume-less particles can be intercepted by the ray, and this model can work together with the Point Particle Model.

2.2 Emission from a Particle

We now focus on the implementation of Monte Carlo methods for the simulation of radiative transfer in particle-based media, i.e., how photon bundles are emitted from the particle field, how they are traced, and how they interacte with other particles.

A small gas volume emits energy uniformly into all directions. In Monte Carlo simulations, the total energy is divided into a number of photon bundles (rays) which are released in random directions. In a physical gas volume, the emitted energy comes from every point in the volume. If the medium is represented by discrete particles, emission takes place inside these particles. Thus, depending on the optical thickness of the particle, and the point and direction of emission, some of the emitted energy may not escape from the particle due to self-absorption. If the particle is optically thin, the self-absorption of emission is negligible and the total emission from particle i is calculated from [1]

$$Q_{emi,i} = 4\kappa_{\rho,i} m_i \sigma T_i^4, \tag{10}$$

where $\kappa_{\rho,i}$ is the density-based absorption coefficient at particle temperature T_i, σ is the Stefan-Boltzmann constant, and m_i is the mass. If self-absorption is considered and the particle is assumed to be a constant density sphere, the total emission from a sphere is obtained from [1]

$$Q_{emi,i} = 4\pi R_{o,i}^2 \sigma T_i^2 \left\{ 1 - \frac{1}{2\tau_{o,i}^2} \left[1 - (1 + 2\tau_{o,i}) e^{-2\tau_{o,i}} \right] \right\}, \tag{11}$$

where $R_{o,i} = (3V_{o,i}/4\pi)^{1/3}$ is the nominal spherical radius of particle i and $\tau_{o,i} = \rho_{o,i} \kappa_{\rho,i} R_{o,i}$ is the optical thickness of the spherical

volume based on the nominal radius. In the Point Particle Model, the shape of a particle is arbitrary, but Eq. (11) is still a good approximation of total emission from such a particle. If more than one ray is emitted from a particle, the sum of initial energy carried by all rays must be equal to the total emission calculated from Eq. (10) or Eq. (11), depending on whether self-absorption is neglected.

2.3 Absorption Models

The basic task of simulating the absorption of a photon bundle in a medium described by a point particle field is the evaluation of the optical thickness that a ray travels through along its way. This is achieved by modeling the interaction between the ray and particles in its path. Based on different models employed for rays and particles, several schemes for absorption simulation may be obtained.

Line-SPM Scheme In this scheme, the ray is treated like a line and the Spherical Particle Model (SPM) is employed for the particles as shown in Fig. 1b. The contribution of particle i to the optical thickness that ray j passes through is computed as

$$\Delta\tau_{ij} = \int_{S_{ij}} \hat{\rho}_i(\mathbf{x}(s))\kappa_{\rho,i}\,\mathrm{d}s, \tag{12}$$

where s is the ray coordinate as in Eq. (7), S_{ij} is the intersection of ray j and the influence region of particle i, $\kappa_{\rho,i}$ is the density-based absorption coefficient of particle i at its own temperature, and $\hat{\rho}_i$ is the local density of particle i as indicated in Fig. 1b. If the Constant Density Sphere (CDS) model is employed, the mass of particle is distributed uniformly in its influence region and Eq. (12) can be simplified to

$$\Delta\tau_{ij} = 2\rho_{o,i}\kappa_{\rho,i}\sqrt{R_i^2 - r_{ij}^2}, \tag{13}$$

where $\rho_{o,i}$ is the nominal density defined in Eq. (3), R_i is the influence radius and r_{ij} is the distance from the center of particle i to ray j. Since Eq. (13) has a very simple form, its implementation can be very fast.

The total optical thickness that ray j passes through is simply the summation of the contributions from the individual particles it interacts with,

$$\tau_j = \sum_{i\in I_j} \Delta\tau_{ij}, \tag{14}$$

where I_j denotes all the particles intersected by ray j.

Cone-PPM Scheme If the ray is modeled as a cone, it is possible to let it interact with point particles. The energy that a conical ray reduces when it traverses over a small distance ds in a continuous medium is,

$$\mathrm{d}E = \int_0^{R_c} \kappa\mathrm{d}sI(r)2\pi r\,\mathrm{d}r = \overline{\kappa}\mathrm{d}s\int_0^{R_c} I(r)2\pi r\,\mathrm{d}r, \tag{15}$$

where κ is the local absorption coefficient, $\overline{\kappa}(s)$ is the plane-averaged absorption coefficient over the cone cross-section at position s, and $R_c(s)$ is the local radius of the cross-section. From Eqs. (15), (7) and (8) the plane-averaged absorption coefficient can be derived as

$$\overline{\kappa} = \frac{\int_0^{R_c}\kappa Ir\,\mathrm{d}r}{\int_0^{R_c} Ir\,\mathrm{d}r} = \frac{\int_0^1 \kappa Ir'\,\mathrm{d}r'}{\int_0^1 Ir'\,\mathrm{d}r'} = \frac{\int_0^1 \kappa W_{2D}2r'\,\mathrm{d}r'}{\int_0^1 W_{2D}2r'\,\mathrm{d}r'} = \int_0^1 \kappa W_{2D}2r'\,\mathrm{d}r' \tag{16}$$

Therefore, the total optical thickness that the ray passes through along in its path S is

$$\begin{aligned}\tau &= \int_S \overline{\kappa}\,\mathrm{d}s = \int_S\int_0^1 \kappa W_{2D}2r'\,\mathrm{d}r'\,\mathrm{d}s \\ &= \int_S\int_0^{R_c} \frac{\kappa W_{2D}}{\pi R_c^2}\,2\pi r\mathrm{d}r\mathrm{d}s = \int_V \frac{\kappa W_{2D}}{\pi R_c^2}\,\mathrm{d}V,\end{aligned} \tag{17}$$

where V is the volume that the ray covers in its path.

In discrete particle fields as shown in Fig. 3a, the absorption coefficient is represented by a set of Delta functions,

$$\kappa = \sum_i \kappa_i V_i \delta(\mathbf{x} - \mathbf{x}_i). \tag{18}$$

Integrating over V yields

$$\tau = \sum_{i\in I} \frac{\kappa_i W_i V_i}{\pi R_{c,i}^2} = \sum_{i\in I} \frac{\kappa_{\rho,i} W_i m_i}{\pi R_{c,i}^2}, \tag{19}$$

where I denotes all the particles enclosed by the cone. For point particles, the particle weight is a point weight in the energy distribution, i.e.,

$$W_i = W_{2D}(r_i/R_{c,i}) = W_{2D}(r_i'), \tag{20}$$

where r_i' is the distance from particle i to the cone axis, normalized by the local cone radius $R_{c,i}$.

Cone-SPM Scheme In the most advanced scheme, the ray is treated as a cone, and the particle is given a specific shape and a density distribution may exist in its volume, as shown in Fig. 3b.

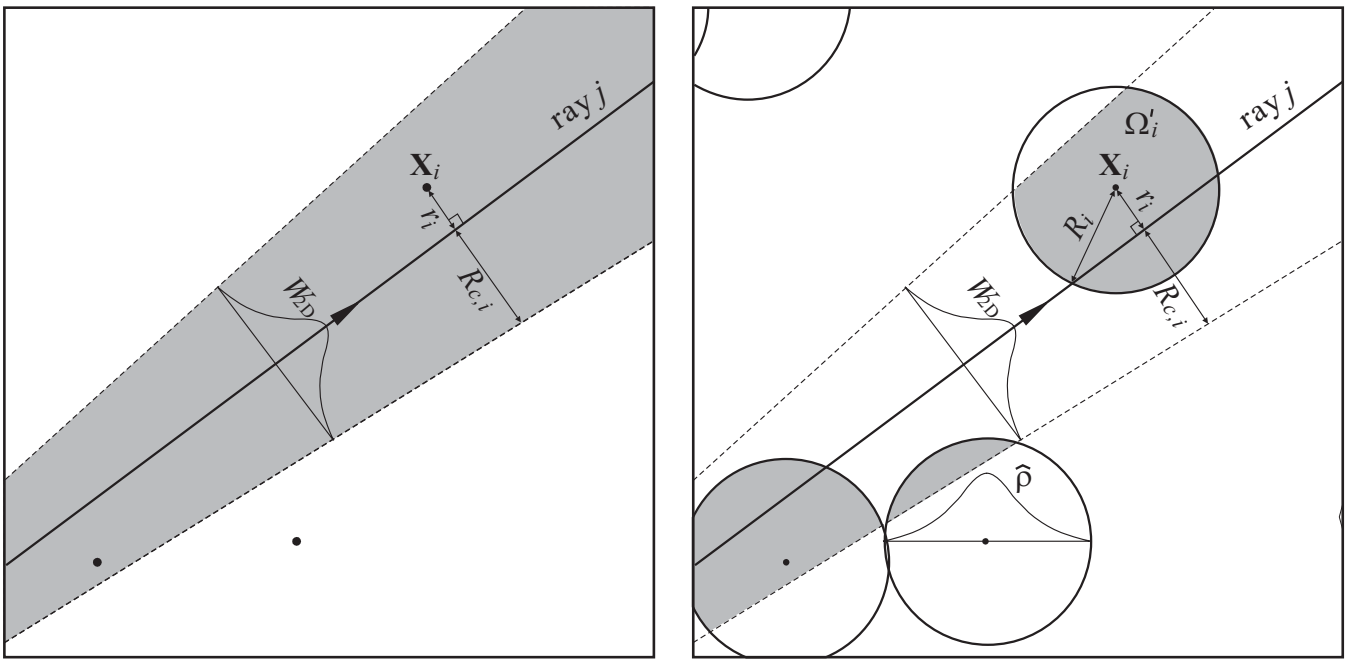

Figure 3. (a) Cone-PPM scheme; (b) Cone-SPM scheme

Therefore, the weight function and absorption coefficient cannot be separated from the volume integral in the optical thickness evaluation. The total optical thickness passed through by a ray is obtained as

$$\tau = \sum_{i\in I} \kappa_{\rho,i} \int_{\Omega'_i} \hat{\rho}_i W_{2D}\left(r/R_c(s)\right) \Big/ \pi R_c^2(s)\, \mathrm{d}\mathbf{x}, \tag{21}$$

where Ω'_i is the intersection of the particle influence region and the ray, r is the distance from a location in Ω'_i to the cone axis and $R_c(s)$ is the local cone radius at this location. Since the solid angle of the ray is small, $R_c(s)$ can be regarded as constant in a single particle, i.e., the small cone segment interacting with a particle can be treated as a small cylinder. Then, the local radius $R_c(s) \equiv R_{c,i}$ can be separated from the integral,

$$\tau \simeq \sum_{i\in I} \frac{\kappa_{\rho,i}}{\pi R_{c,i}^2} \int_{\Omega'_i} \hat{\rho}_i(\mathbf{x}) W_{2D}\left(r/R_{c,i}\right)\, \mathrm{d}\mathbf{x}. \tag{22}$$

For constant-density spherical particles this reduces to

$$\begin{aligned} \tau &= \sum_{i\in I} \frac{\kappa_i}{\pi R_{c,i}^2} \int_{\Omega'_i} W_{2D}(r/R_{c,i})\, \mathrm{d}\mathbf{x} \\ &= \sum_{i\in I} \frac{\kappa_i}{\pi R_{c,i}^2} \int_{r_{min}}^{r_{max}} W_{2D}(r/R_{c,i}) A_i(r)\, \mathrm{d}r, \\ &= \sum_{i\in I} \frac{\kappa_i R_{c,i}}{\pi} \int_{r'_{min}}^{r'_{max}} W_{2D}(r') A'_i(r')\, \mathrm{d}r', \end{aligned} \tag{23}$$

where $r' = r/R_{c,i}$ is the normalized distance from a point in Ω'_i to the cylinder (cone) axis. r'_{min} is the normalized closest distance and r'_{max} is the farthest. All points of the same distance r' are part of a cylindrical shell $A_i(r')$ around the cone axis, and its normalized form can be evaluated as

$$A'_i(r') = \frac{A_i(r')}{R_{c,i}^2} = \begin{cases} 4r'^{3/2} r_i'^{1/2} \alpha^{1/2} E(1/\alpha), & r' \le R'_i - r'_i \\ 8r'^{3/2} r_i'^{1/2} [2E(\alpha) - \beta K(\alpha)], & r' > R'_i - r'_i \end{cases}, \tag{24}$$

where $r'_i = r_i/R_{c,i}$ is the normalized distance from the particle center to the cylinder axis, $R'_i = R_i/R_{c,i}$ is the normalized radius of particle i, K and E are complete elliptic integrals of the 1^{st} and 2^{nd} kind [17], and

$$\begin{aligned} \alpha &= [R_i'^2 - (r' - r'_i)^2]/4r' r'_i, \\ \beta &= [(r' + r'_i)^2 - R_i'^2]/2r' r'_i. \end{aligned} \tag{25}$$

If we define

$$f_i = \frac{1}{\pi} \int_{r'_{min}}^{r'_{max}} W_{2D}(r') A'_i(r') \, \mathrm{d}r', \tag{26}$$

Eq. (23) can be rewritten as

$$\tau = \sum_{i \in I} \kappa_i R_{c,i} f_i. \tag{27}$$

Rather than making costly evaluations during the simulation, Eq. (26) can easily be tabulated as a function of the two dimensionless parameters r'_i and R'_i.

3 Sample Calculations

In order to evaluate and compare the performance of the different schemes for Monte Carlo ray tracing in particulate media, we consider a one-dimensional radiative heat transfer problem, in which a non-scattering gray gas slab is bounded by two parallel cold black plates which are 10 cm apart. The temperature and density (or absorption coefficient) may vary in the x-direction. The resulting radiative heat flux at the boundary can be evaluated analytically as [1]

$$\begin{aligned} q(0) &= -2\pi \int_0^{\tau_L} I_b(\tau') E_2(\tau') \, \mathrm{d}\tau' \\ q(\tau_L) &= 2\pi \int_0^{\tau_L} I_b(\tau') E_2(\tau_L - \tau') \, \mathrm{d}\tau', \end{aligned} \tag{28}$$

where E_2 is an exponential integral and the optical thickness τ is a function of x,

$$\tau(x) = \int_0^x \kappa(x) \, \mathrm{d}x \quad \text{and} \quad \tau_L = \int_0^L \kappa(x) \, \mathrm{d}x, \tag{29}$$

and $L = 10$ cm is the distance between two parallel plates.

The one-dimensional medium in the problem can be simulated by repeating a gas cube, each with equal side-lengths of 10 cm in the other two infinite dimensions. A single gas cube is then the computational domain in the Monte Carlo simulation. The gas in the cube is represented by a number of discrete gas particles randomly placed inside the cube. The mass of particles may be equally-sized or have a distribution along the x-direction. For computational efficiency, the domain is further broken up into cubic cells, each of which contains a number of gas particles. Some of the particles are completely inside the cell, and the others have a part of their volume reside in the neighboring cell. If the Point Particle Model (PPM) is employed, it can be assumed that all the particles are completely enclosed by the cell, since the shape of particles is not specified. However, if the Spherical Particle Model (SPM) or the Constant Density Sphere (CDS) model is employed, the cell contains not only the particles with their center in it, but also parts of particles from neighboring cells. Thus, a scheme must be developed to avoid having the ray interact with a single particle more than once, since a single particle may belong to multiple cells.

When the Cone Ray Model is adopted for ray tracing, the opening angle (the angle between the cone axis and the lateral surface) needs to be chosen. Larger opening angles result in more particles caught by the ray, requiring more CPU time per ray but providing better accuracy. It was found that, for this one-dimensional problem, one degree was an optimal opening angle, which can achieve high accuracy as well as high CPU efficiency. Therefore, for all the simulations in this paper, the opening angle is chosen to be one degree, whenever the Cone Ray Model is employed.

Several combinations of temperature profiles and absorption coefficient profiles have been tested as listed in Table 1, with different cases numbered in Table 2. For each of the nine cases, two different particle volume distributions as given in Table 3 were tested. In the uniform distribution, the particles are equally-sized and their random positions in the computational domain can be readily generated as

$$x = \eta_x L, \; y = \eta_y L, \; z = \eta_z L, \tag{30}$$

where η_x, η_y and η_z are three independent random numbers uniformly distributed in $[0, 1)$. For the linear distribution of particle mass, the random number relation for the x-coordinate of particle positions is no longer linear. Instead, the probability distribution $P(x)$ associated with particle mass distribution $m(x)$ is inversely

Table 1. Temperature and absorption coefficient profiles

Temperature profiles, K	
const	$T(x) = T_o$
linear	$T(x) = T_o + (x/L)(T_L - T_o), \quad T_L/T_o = 2$
sine	$T(x) = T_o + T_A \sin(2\pi x/L), \quad T_A/T_o = 0.5$
Absorption coefficient profiles, cm^{-1}	
const	$\kappa(x) = 0.1$
linear	$\kappa(x) = 0.01 + 0.99(x/L)$
sine	$\kappa(x) = 0.55 + 0.45\sin(2\pi x/L)$

Table 3. Particle mass distributions

uniform	$m(x) = m_o$
linear	$m(x) = m_o + (m_L - m_o)(x/L)$

Table 2. Case numbering

Case	(1)	(2)	(3)	(4)	(5)	(6)	(7)	(8)	(9)
T	const	const	const	linear	linear	linear	sine	sine	sine
κ	const	linear	sine	const	linear	sine	const	linear	sine

proportional to $m(x)$, i.e., $P(x) \sim 1/m(x)$. Therefore, the following random number relation holds,

$$\eta_x = \frac{\int_0^x P(x)\,\mathrm{d}x}{\int_0^L P(x)\,\mathrm{d}x} = \frac{\int_0^x 1/m(x)\,\mathrm{d}x}{\int_0^L 1/m(x)\,\mathrm{d}x} = \frac{\int_0^x [m_o + (m_L - m_o)(x/L)]^{-1}\,\mathrm{d}x}{\int_0^L [m_o + (m_L - m_o)(x/L)]^{-1}\,\mathrm{d}x}. \tag{31}$$

After carrying out the integrations and rearranging, one obtains

$$x = \frac{(m_L/m_o)^{\eta_x} - 1}{(m_L/m_o) - 1} L, \tag{32}$$

where (m_L/m_o) is the mass ratio of particles at $x = L$ to particles at $x = 0$. Figure 4 shows a CDS representation with a linear particle mass distribution for a homogeneous medium.

The three absorption schemes discussed in Section 2 have been implemented for the 1D problem and compared with the exact solution for boundary fluxes, Eq. (28), for all nine cases. Table 4 shows the corresponding root-mean-square (RMS) relative error of 50 simulations in each case, in which the gas cube is represented by 10,000 equally-sized random particles each of which emits all its energy in a single ray into a random direction. Similarly, Table 5 gives the results for the linear particle mass distribution. In both tables, the computational domain is divided into 4 cells in each dimension, 64 cells in total. For all nine cases, the same random number sequence is used in the particle position generation as well as in the emission direction generation. As shown in the two tables, the three absorption schemes all achieve the same level of accuracy. Comparing Table 5 to Table 4, it is observed that the difference caused by varying the particle masses is fairly small considering that the mass ratio is as large as 1,000.

From the above comparisons, one may conclude that the three absorption schemes are essentially equivalent in terms of simulation accuracy. Therefore, in the following accuracy-related discussions, we choose only one scheme, the Line-CDS scheme, to show the results.

The errors of fluxes at the two boundaries are averaged and plotted in Fig. 5 against the number of particles by which the

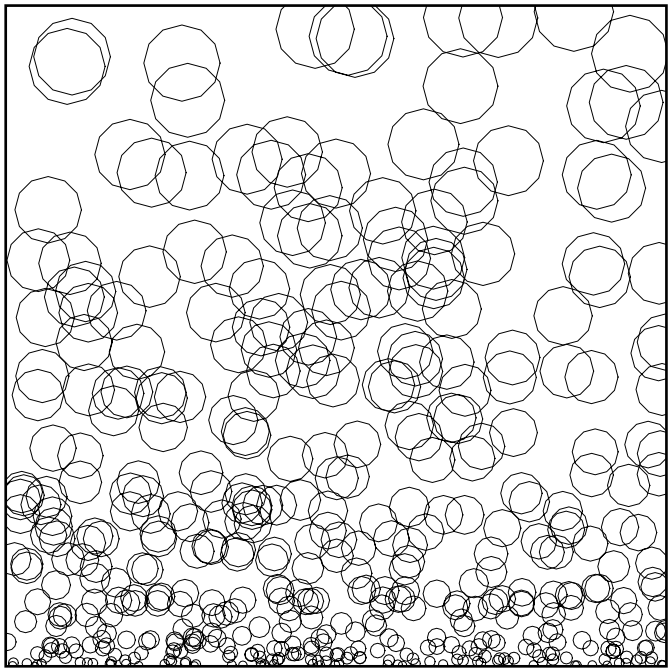

Figure 4. CDS representation with linear mass distribution for a homogeneous medium

Table 4. Percentage RMS errors of radiative fluxes at boundaries; 10,000 particles; 1 ray/particle; 64 cells; uniform particle mass

Case	Line-CDS		Cone-PPM		Cone-CDS	
No.	$x = 0$	$x = L$	$x = 0$	$x = L$	$x = 0$	$x = L$
(1)	1.457	1.508	1.845	1.940	1.485	1.572
(2)	1.274	1.555	1.288	1.665	1.282	1.586
(3)	1.673	1.593	1.820	1.592	1.676	1.592
(4)	2.144	1.890	3.353	1.862	1.635	1.993
(5)	1.612	2.028	1.674	1.999	1.624	2.104
(6)	1.883	1.711	3.433	1.673	2.302	1.696
(7)	1.957	2.159	1.985	3.131	2.016	1.990
(8)	1.718	1.792	1.686	2.223	1.714	1.749
(9)	2.084	2.087	2.012	2.072	2.109	2.150

Table 5. Percentage RMS errors of radiative fluxes at boundaries; 10,000 particles; 1 ray/particle; 64 cells; mass ratio: $m_L/m_o = 1,000$

Case	Line-CDS		Cone-PPM		Cone-CDS	
No.	$x = 0$	$x = L$	$x = 0$	$x = L$	$x = 0$	$x = L$
(1)	1.896	3.378	2.231	3.776	1.956	3.113
(2)	2.795	3.671	2.823	3.772	2.776	3.633
(3)	1.863	2.234	1.989	2.243	1.816	2.089
(4)	4.050	4.332	5.138	4.403	3.606	4.501
(5)	4.584	4.740	4.700	4.803	4.510	4.863
(6)	3.748	3.990	5.274	3.926	4.181	3.930
(7)	2.174	4.412	2.062	5.574	2.217	2.723
(8)	2.398	3.647	2.400	4.131	2.385	2.945
(9)	2.377	2.487	2.217	2.566	2.335	2.361

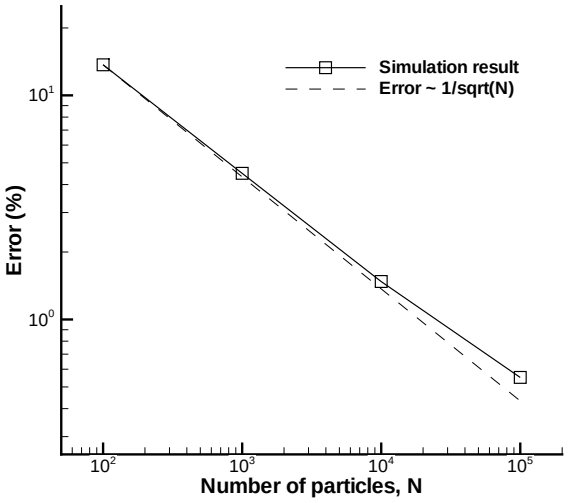

Figure 5. Averaged boundary flux error vs. number of particles in computation domain; Line-CDS scheme with one ray per particle; uniform particle mass; Case (1)

medium in the gas cube is represented. The particles are all of the same size and only the result of Case (1) is provided for simplicity. It is seen that the error is approximately inversely proportional to the square root of the number of particles. Similarly, Fig. 6 shows the relation of error and the number of rays that each particle emits during the Monte Carlo simulation, given the number of particles. Once again, the accuracy follows an inverse square root relation.

All three absorption models achieve not only the same level

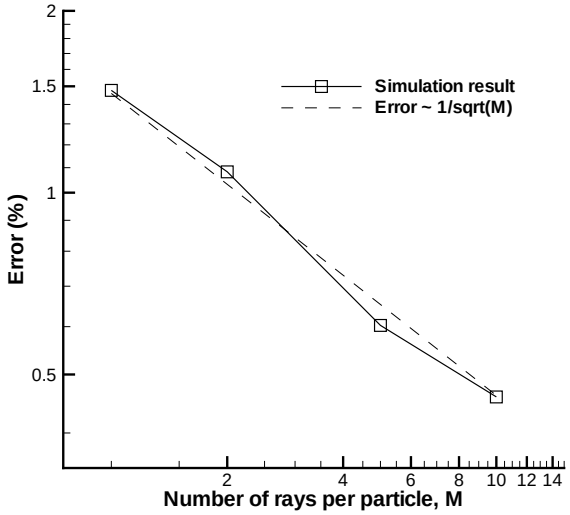

Figure 6. Averaged boundary flux error vs. number of rays per particle; Line-CDS scheme; 10,000 particles; uniform particle mass; Case (1)

Table 6. CPU time of a single Monte Carlo simulation; 1 ray/particle; Case (1); unit: s

Particle amount	2,000	5,000	10,000	50,000	100,000
Number of cells	2^3	3^3	4^3	7^3	8^3
Line-CDS	0.115	0.417	1.29	48.7	183.2
Cone-PPM	0.230	0.742	1.98	56.4	215.7
Cone-CDS	0.231	0.752	2.07	58.1	214.9

of accuracy, but also similar CPU efficiency for this 1D problem, as shown in Table 6. The Line-CDS scheme is a little bit faster than the other two, since a line ray interacts with fewer particles than a cone ray, but due to the small opening angle of the Cone Ray Model, the time difference is not very big.

4 Conclusions

For radiative heat transfer simulations using Monte Carlo ray tracing in media represented by discrete particle fields it is important to find a way to model the interaction between point-masses and photon rays. In the Point Particle Model (PPM) the shape of particles is not presumed in order to avoid any inconsistency with the original particle field. As a result, it is limited to applications in which the ray has a shape and volume. In the Spherical Particle Model (SPM), particles are assumed to be spheres. As a special case, in the Constant Density Sphere (CDS) model, the density is assumed to be constant across the entire particle volume. Although it is easy to interact spheres with a ray,

this model introduces some inconsistencies. For example, it cannot recover continuous medium properties due to the existence of particle overlaps and void.

In the Line Ray Model for a photon bundle, the ray is simply treated as a volume-less line and energy propagates one-dimensionally along that line. In the Cone Ray Model, the ray is assigned a small solid angle, and is thus treated as a cone; energy propagates two-dimensionally. The strength of the ray may vary across the cross-section of the cone through a given weight function. Since the ray has a volume, it is possible to have the ray interact with volume-less particles directly. Thus, three schemes for the interaction between ray and particles, i.e., Line-CDS, Cone-PPM and Cone-CDS schemes, have been proposed and examined in a one-dimensional radiative heat transfer problem with various temperature and absorption coefficient profiles. It was shown that all three schemes achieved comparable levels of accuracy and CPU-time efficiency.

Acknowledgment

This research has been sponsored by National Science Foundation under Grant Number CTS-0121573.

References

[1] Modest, M. F., 2003, *Radiative Heat Transfer*, Academic Press, New York, 2nd ed.

[2] Heinisch, R. P., Sparrow, E. M., and Shamsundar, N., 1973, "Radiant Emission from Baffled Conical Cavities", *Journal of the Optical Society of America*, **63**(2), pp. 152–158.

[3] Shamsundar, N., Sparrow, E. M., and Heinisch, R. P., 1973, "Monte Carlo Solutions — Effect of Energy Partitioning and Number of Rays", *International Journal of Heat and Mass Transfer*, **16**, pp. 690–694.

[4] Modest, M. F. and Poon, S. C., 1977, "Determination of Three-Dimensional Radiative Exchange Factors for the Space Shuttle by Monte Carlo", ASME paper no. 77-HT-49.

[5] Modest, M. F., 1978, "Determination of Radiative Exchange Factors for Three Dimensional Geometries with Nonideal Surface Properties", *Numerical Heat Transfer*, **1**, pp. 403–416.

[6] Walters, D. V. and Buckius, R. O., 1992, "Monte Carlo Methods for Radiative Heat Transfer in Scattering Media", In *Annual Review of Heat Transfer*, **5**, Hemisphere, New York, pp. 131–176.

[7] Modest, M. F., 2003, "Backward Monte Carlo Simulations in Radiative Heat Transfer", *ASME Journal of Heat Transfer*, **125**(1), pp. 57–62.

[8] Howell, J. R., 1998, "The Monte Carlo Method in Radiative Heat Transfer", *ASME Journal of Heat Transfer*, **120**(3), pp. 547–560.

[9] Farmer, J. T. and Howell, J. R., 1998, "Monte Carlo strategies for radiative transfer in participating media", In Hartnett, J. P. and Irvine, T. F., eds., *Advances in Heat Transfer*, **34**, Academic Press, New York.

[10] Tessé, L., Dupoirieux, F., Zamuner, B., and Taine, J., 2002, "Radiative transfer in real gases using reciprocal and forward Monte Carlo methods and a correlated-k approach", *International Journal of Heat and Mass Transfer*, **45**, pp. 2797–2814.

[11] Tessé, Lionel, Dupoirieux, Francis, and Taine, Jean, 2004, "Monte Carlo modeling of radiative transfer in a turbulent sooty flame", *International Journal of Heat and Mass Transfer*, **47**, pp. 555–572.

[12] Pope, S. B., 1985, "PDF Methods for Turbulent Reactive Flows", *Progress in Energy and Combustion Science*, **11**, pp. 119–192.

[13] Dopazo, C., 1994, "Recent developments in pdf methods", In *Turbulent Reacting Flows*, Academic Press, pp. 375–474.

[14] Li, G. and Modest, M. F., 2002, "Investigation of Turbulence–Radiation Interactions in Reacting Flows Using a Hybrid FV/PDF Monte Carlo Method", *Journal of Quantitative Spectroscopy and Radiative Transfer*, **73**(2–5), pp. 461–472.

[15] Raman, V., Fox, R. O., and Harvey, A. D., 2004, "Hybrid finite-volume/transported PDF simulations of a partially premixed methane–air flame", *Combustion and Flame*, **136**, pp. 327–350.

[16] Liu, G. R. and Liu, M. B., 2003, *Smoothed Particle Hydrodynamics – a Meshfree Particle Method*, World Scientific Publishing Co. Pte. Ltd., Singapore.

[17] Abramowitz, M. and Stegun, I. A., eds., 1965, *Handbook of Mathematical Functions*, Dover Publications, New York.